Physics in Medicine &
Biology

NOTE

A clustering tool for generating biological geometries for computational modeling in radiobiology

To cite this article: Ramon Ortiz and José Ramos-Méndez 2024 *Phys. Med. Biol.* **69** 21NT01

IOP Publishing Phys. Med. Biol. 69 (2024) 21NT01 https://doi.org/10.1088/1361-6560/ad7f1d

Physics in Medicine & Biology

IPEM Institute of Physics and Engineering in Medicine

NOTE

A clustering tool for generating biological geometries for computational modeling in radiobiology

Ramon Ortiz and José Ramos-Méndez*

University of California San Francisco, Department of Radiation Oncology 1600 Divisadero Street, San Francisco, CA 94143, United States of America

* Author to whom any correspondence should be addressed.

E-mail: jose.ramosmendez@ucsf.edu

RECEIVED
2 July 2024

REVISED
17 September 2024

ACCEPTED FOR PUBLICATION
24 September 2024

PUBLISHED
11 October 2024

Keywords: monte carlo modeling, radiobiology, clustering, segmentation images, agent-based software

Abstract

Objective. To develop a computational tool that converts biological images into geometries compatible with computational software dedicated to the Monte Carlo simulation of radiation transport (TOPAS), and subsequent biological tissue responses (CompuCell3D). The depiction of individual biological entities from segmentation images is essential in computational radiobiological modeling for two reasons: image pixels or voxels representing a biological structure, like a cell, should behave as a single entity when simulating biological processes, and the action of radiation in tissues is described by the association of biological endpoints to physical quantities, as radiation dose, scored the entire group of voxels assembling a cell. *Approach.* The tool is capable of cropping and resizing the images and performing clustering of image voxels to create independent entities (clusters) by assigning a unique identifier to these voxels conforming to the same cluster. The clustering algorithm is based on the adjacency of voxels with image values above an intensity threshold to others already assigned to a cluster. The performance of the tool to generate geometries that reproduced original images was evaluated by the dice similarity coefficient (DSC), and by the number of individual entities in both geometries. A set of tests consisting of segmentation images of cultured neuroblastoma cells, two cell nucleus populations, and the vasculature of a mouse brain were used. *Main results.* The DSC was 1.0 in all images, indicating that original and generated geometries were identical, and the number of individual entities in both geometries agreed, proving the ability of the tool to cluster voxels effectively following user-defined specifications. The potential of this tool in computational radiobiological modeling, was shown by evaluating the spatial distribution of DNA double-strand-breaks after microbeam irradiation in a segmentation image of a cell culture. *Significance.* This tool enables the use of realistic biological geometries in computational radiobiological studies.

1. Introduction

The response of living organisms to different agents can be studied with different software dedicated to simulating both the physical action of an agent and the subsequent biological processes (Brodland 2015). An example of such application is computational modeling in radiobiology and radiotherapy, where the study of the effects of ionizing radiation on tissues is of high importance.

Different software have been extensively used in this field to simulate the physical interactions of radiation with matter, and the subsequent biological responses. For example, the TOPAS Monte Carlo tool (Perl *et al* 2012, Faddegon *et al* 2020), and its Monte Carlo track-structure extension TOPAS-nBio (Schuemann *et al* 2018), both built on the top of the Geant4 toolkit, have been used to compute physical and chemical quantities relevant to biological endpoints (Ramos-Méndez *et al* 2021, Faddegon *et al* 2023). On the other hand, CompuCell3D (CC3D) (Swat *et al* 2012) has been used for the simulation of radiobiological processes, such as the tumor response after irradiation, among many other applications (Liu *et al* 2021).

TOPAS-nBio includes a limited set of generic cellular (e.g. spherical, ellipsoid, and fibroblasts cells) and subcellular (e.g. plasmids, linear DNA, solenoid chromatin fiber or spherical mitochondria) geometries (McNamara *et al* 2018). CC3D can generate from simplistic to complex geometries, such as a spherical collection of voxels representing cells or voxelized cells with irregular topology. Both software allow importing geometries in different formats, e.g. Potts initialization format (PIF) format in CC3D and binary (ImageCube) or DICOM format in TOPAS/TOPAS-nBio. The PIF format consists of a set of entries that define each entity (e.g. a cell) or site in the simulation lattice. The entries typically are a cell ID, the cell name, and the spatial coordinates defining the position of the cell in the simulation lattice. The ImageCube refers to a binary file that contains one identifying value for each voxel that can be associated with a material. These methods can be used to accurately represent specific experimental geometries, such as the shape and spatial distributions of cells in a specific experimental assay. However, the generation of specific complex voxelized geometries in PIF or ImageCube format is a challenging task due to the large amount of data (i.e. voxels) conforming those geometries, limiting this task to researchers with programming experience. Furthermore, geometries created from biological images, even when imported as DICOM, PIF or ImageCube formats, have voxels with their own independent agency rather than being associated with a group of voxels to define individual entities, such as cells or cellular nuclei.

Modeling the effects of ionizing radiation in living organisms (group of cells) can be described by an association of physical, chemical and radiobiological quantities with a biological endpoint in a cellular or subcellular basis. In other words, a given biological endpoint is typically associated with the value of a dosimetric quantity in the entire cellular or subcellular structure. For instance, the number of radiation-induced cellular DNA double-strand breaks (DSB) can be associated with the mean microdosimetric specific energy scored an irradiated cell nucleus (Thibaut *et al* 2023); the vascular damage can be derived from the mean dose scored from individual vascular cells (Garcia-Barros *et al* 2003). Thus, in computational studies for radiobiology, the identification and depiction of these individual entities, assembled from a subset of voxels in biological images (e.g. by clustering) is required in to evaluate a given physical dosimetric quantity in each of those individual biological structures.

In this work we present a computational tool that performs the clustering of voxels of biological images into user-defined entities (e.g. cells of a given size). The tool produces files with geometries in PIF and ImageCube formats compatible with CC3D and TOPAS/TOPAS-nBio simulation tools. The tool facilitates the coupled simulation using both software, from the radiation energy deposition to the cell fate. In addition, this tool can perform the cropping and resolution resizing of the images following user input to improve the computational efficiency of simulations. The performance of the interface tool is assessed for a set of experimental images relevant for radiobiology and by comparing the generated geometries to the original images via the dice similarity coefficient (DSC). Finally, as an example of application, we compute the distribution of DSB in a cell population after irradiation with x-ray microbeams.

2. Materials and methods

2.1. Description of the tool

The tool is composed of three modules that perform the *cropping* of the original image, *resizing* the resolution of the original/cropped image, and *clustering* the voxels of the original/cropped/resized image. In addition, two modules save the geometry of the images in PIF and ImageCube format. The communication of all these modules and user input functions are managed by the *main* module. All modules, except for the clustering one, which is written in C++ (v.14), are written in Python (v.3.11).

The information required by the tool can be input by the user via a graphical user-interface, built with Python-Tk, or as an ASCII file. This information is:

1. Directory path to the original image. The current version of the tool is compatible with TIFF, NII, and DICOM formats. Two- and three-dimensional images are supported.
2. The threshold value for the segmentation of the image, i.e. image intensity threshold.
3. A boolean flag (Yes or No options) to perform the cropping of the image.
4. The dimensions in the number of pixels or voxels of the cropped image.
5. The initial vertex (pixel/voxel location) in the image for cropping.
6. A boolean flag (Yes or No options) to perform the resizing of the image.
7. The resizing factor, i.e. an integer factor to crop the number of voxels in each direction.
8. A boolean flag (Yes or No options) to perform the clustering of voxels.
9. The minimum and maximum cluster volume (in total number of pixels or voxels).
10. The name of the clustered structure, e.g. Neuron.
11. The path to the output directory.

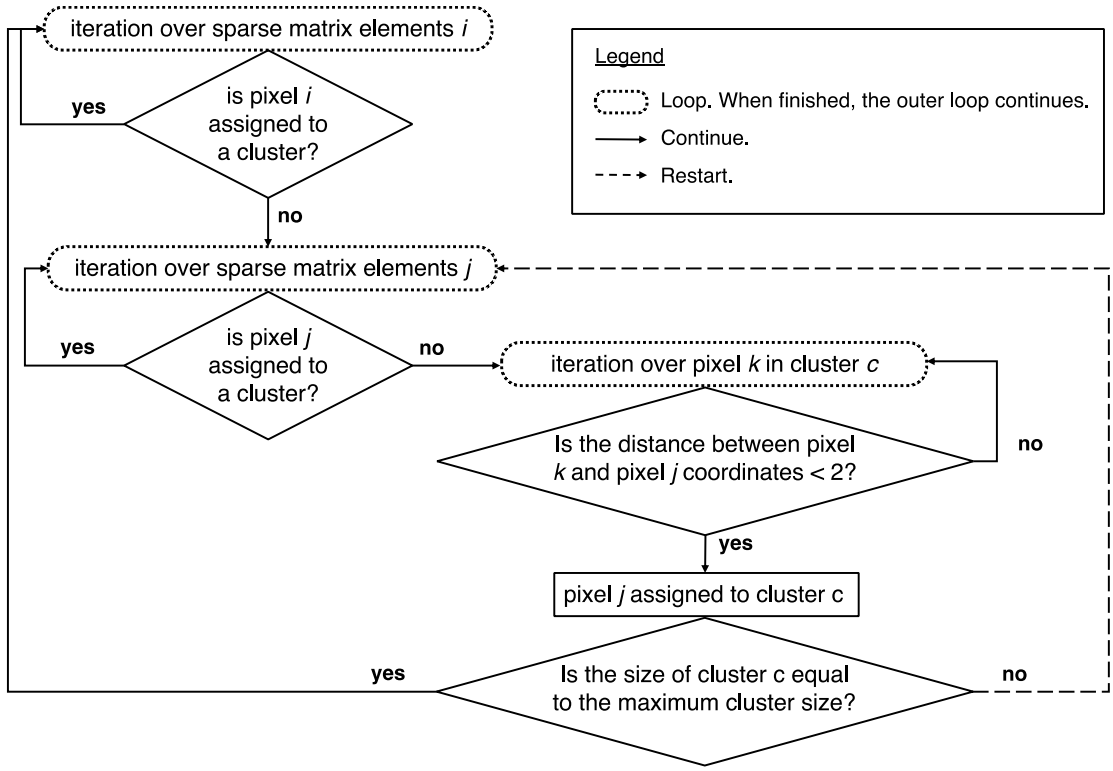

Figure 1. Workflow of the clustering algorithm.

This information is used by the tool as follows. The image in NII, TIFF, and DICOM format is read using NiBabel, Pyplot, and PyDICOM libraries, respectively. The data is saved in a NumPy matrix. This matrix is cropped by the cropping module following the user specifications. The resizing is performed following user input parameters with the SciPy library. The clustering process is performed by the clustering module as follows. A sparse matrix is created considering the image voxels with a value higher than the threshold value for segmentation provided by the user. This matrix contains the coordinates of each voxel. A given voxel i is assigned to the cluster c. The distance (in the image coordinates) between the voxels conforming the cluster c and the other voxels j is determined, and if they are adjacent (i.e. distance of 1), then they are assigned to the same cluster. Each time a voxel j is assigned to a cluster, the iteration over the matrix elements j is restarted to consider the increment in volume of the cluster as voxels are assigned to it and the potential proximity of an already evaluated voxel j to the new cluster volume. When all the elements j are evaluated, or the cluster size reaches the maximum number of voxels per cluster, the process is started over for another cluster. In all these steps, only voxels not assigned previously to another cluster are considered. A representation of the clustering algorithm is shown in figure 1. Clusters of size lower than the minimum cell volume (specified by the user) will not be considered to create the new geometry.

The data generated in each of the modules (i.e. cropping, resizing, and clustering) is used as input by the subsequent module. The generated data is written in PIF and ImageCube formats and saved in the specified output directory. In PIF files, each line corresponds to a voxel and contains columns describing the cluster index, the name of the cell type it belongs to, and its XYZ coordinates in the lattice. ImageCube files consist of a voxelized lattice, and each voxel contains the cluster index it belongs to. An ASCII parameter file is also created for ready-to-run TOPAS simulations. In these files, voxels belonging to the same cluster (i.e. cell or nucleus) were assigned a unique integer identifier (i.e. a cluster index). A unique identifier per entity ensures (i) compatibility with TOPAS. In this way, the physical dosimetric quantity scored at each voxel will be assigned to the biological structure (e.g. cell or cell nucleus) they belong to for the association of this quantity to a given biological endpoint, typically defined per cell or cell nucleus, and (ii) that, in CC3D, all voxels conforming each cell will behave in a coordinate manner in the simulation of biological processes such as damage repair or cell growth, division and death.

2.2. Evaluation of the tool performance

To evaluate the performance of the tool to cluster voxels in the original images into individual entities (e.g. cells), four relevant sets of data in radiobiology research applications were used:

Table 1. Summary of the parameters used for Test 1–5. *Coordinates (in voxels) to crop the center of the right hemisphere of the mouse brain. **Average size of the synthetic nuclei. ***500 voxels in this image correspond to a volume of 13 500 μm^3, chosen to resemble the size of vascular cells reported in literature (Félétou 2011).

Parameter	Test 1	Test 2	Test 3	Test 4	Test 5
Dataset	A	B	C	D	A
Segmentation threshold value	0.0	278.0	0.0	0.0	0.0
Performed cropping?	No	No	No	Yes	No
Dimensions of cropped image	—	—	—	(167, 167, 33) *	—
Initial vertex	—	—	—	(700, 1200, 750) *	—
Performed resizing?	No	No	No	No	Yes
Resizing factor	—	—	—	—	2
Performed clustering?	Yes	Yes	Yes	Yes	Yes
Max. cluster volume	None	None	380 **	500 ***	None

A. 2D segmentation images of in vitro cultured neuroblastoma cells,
B. 2D segmentation images of the nuclei of in vitro cultured neuroblastoma cells,
C. 2D fluorescence cell nuclei segmentation images, and
D. 3D segmentation images of the vasculature of a whole mouse brain.

The three first sets correspond to biological images at cellular level acquired by means of epifluorescence microscopy (Dataset A and B), and fluorescence microscopy (Dataset C). These images were taken from the CIL database (Ruusuvuori 2011, Yu Weimiao 2019). The fourth dataset, taken from the VesSAP database (Todorov *et al* 2020), includes vascular segmentation images acquired by light-sheet microscopy imaging of whole mouse brains perfused with wheat germ agglutinin and evans blue dyes.

Five tests were performed using these datasets. In Test 1, Test 2, Test 3 and Test 4, the clustering process was performed for the images A, B, C, and D, respectively. In Test 5, the resizing was performed in addition to the clustering for image A. Table 1 summarizes the input parameter used.

The geometries in the original image and the one generated by the tool (i.e. generated PIF files) were compared using the DSC (Dice 1945). DSC is a statistical measure widely used to assess the similarity between two sets of data, such as the overlap between two segmentation masks (Zou *et al* 2004). DSC ranges from 0, indicating completely dissimilar images, to 1, indicating identical images. It is defined as twice the number of voxels that are common to two segmentation images divided by the sum of the number of voxels in each set:

$$\mathrm{DSC} = \frac{2\,|S1 \cap S2|}{|S1| + |S2|}. \tag{1}$$

The original image and the final geometry generated by the tool (i.e. post-segmentation and clustering processes) were compared. The segmentation threshold (see table 1) was applied to both original and generated images. Thus, DSC allowed to evaluate not only the segmentation process but also the process of clustering, and the correct transformation of coordinates from the original images to TOPAS and CC3D coordinate systems.

In addition, the number of cells or nuclei in the original segmentation images and generated geometries were compared. The number of entities in original images (cells in Dataset A and C, and cellular nuclei in dataset B) was determined by manual cell counting performed by three independent observers. The number of entities in the generated images (i.e. voxel clusters) was the number of unique cell indexes in the generated PIF files. The voxel clusters, created according to the parameters used in each test (see table 1), represent the individual entities in the original images (i.e. cells or nuclei).

2.3. Example of application: DSB distribution after microbeam radiotherapy (MRT) irradiation

To illustrate the application of the developed tool in radiobiology research, we evaluated a scenario where the interplay between dose delivery and spatial distribution of individual cells may determine a given biological endpoint, and thus, the identification of cell shape and dimension (i.e. voxels conforming the cell) is necessary. In particular, we computed the distribution of the DSB in a cell population after MRT (Slatkin *et al* 1992). MRT uses micrometer-size planar beams spatially separated by a certain distance in the micrometer range. This technique produces highly heterogeneous dose distributions, i.e. high-dose areas called peaks and low-dose areas called valleys. Such dose heterogeneity may lead to a non-uniform distribution of DSB in a cell population or tissue. We evaluated the DSB per cell in the vitro cell population of dataset C. The induction of DSB can be associated with the average absorbed dose and linear energy transfer (LET) in the cell nucleus (Belov *et al* 2015), making necessary the clustering of image voxels into individual nuclei.

The geometry generated by the clustering tool, in ImageCube format, was imported to TOPAS for the scoring of the dose per cell nucleus. The irradiation geometry used was a set of 50 μm-wide and 1 mm-long x-ray microbeams separated by 200 μm center-to-center distance, as used in in-vitro experiments (Burger *et al* 2017). The radiation dose, defined as the mean dose in the entire irradiated sample, was 2 Gy. The energy spectrum and lateral beam divergence (0.5 mrad) of the biomedical beamline of the European synchrotron radiation facility (Grenoble, France) in microbeam mode were used (Zhang and Mayr 2023). The TOPAS version used in this work was OpenTOPAS version 4.0, available in the TOPAS collaboration GitHub repository (https://github.com/OpenTOPAS). This version of the TOPAS code is a continuous development from TOPAS version 3.9.

The corresponding cell lattice geometry, in PIF format, was imported to CC3D version 4.2.5, to assign the number of DSB in each cell nucleus as function of the dose calculated in TOPAS. The number of DSB was randomly sampled from a Poisson distribution (Rothkamm and Löbrich 2003) with a mean value of 27.5 DSB/Gy (Belov *et al* 2015).

3. Results

3.1. Evaluation of the tool performance

A visual comparison of the original segmentation images and the geometries generated by the clustering tool is presented in figure 2. The generated geometries are shown using the CC3D and TOPAS visualization, proving the compatibility of the produced PIF and ImageCube file formats with these software.

The DSC between the original images and generated geometries was 1.0 for all the tests performed, indicating that both geometries were identical. The DSC was not evaluated in Test 5 since the image was resized and thus both geometries had different dimensions. The number of individual entities (i.e. cells or nuclei) in the original image and the clusters formed by the clustering tool agreed, confirming its ability to identify individual entities based on user specifications (table 1). The comparison between the number of entities was not performed for Test 4 because the number of cells in the original vasculature segmentation image could not be determined. Table 2 summarizes the quantitative comparison of the original and generated geometries.

Once various geometries were created, the tool combined them to create more complex configurations by merging the PIF files (i.e. appending one to another), while keeping the cluster of compartments to create compartmental CC3D simulations. As a demonstration, we combined datasets A and B to create a geometry containing individual volumes (clusters) representing the cytoplasm and nucleus of each cell. Dataset A was a segmentation image of neuroblastoma cells and dataset B was the corresponding segmentation image of the cell nuclei. We performed the voxel clustering of each image individually (see the parameters used in table 1). Image B was resized by a factor two to match the dimensions of image A (from 1392 $\times$ 1040–692 $\times$ 520 voxels). Then, the generated geometry of dataset B was merged to the generated geometry of dataset A. Figure 3 shows the resulting geometry of the combined PIF file using the CC3D visualization.

The simulation time to create the geometries considered in this work ranged from 42 min to 8 d using a single CPU Apple M2. The simulation time depended on the number of voxels above the segmentation threshold rather than the dimensions of the lattice. The reason for this dependence consisted in that only the voxels above the threshold value were included in the sparse matrix used in the loop to determine the distances between voxels in the clustering process. In addition, the simulation time increased with the cluster volume because the loop over the sparse matrix elements was restarted each time a new element was inserted (see clustering workflow in figure 1). For instance, the simulation time in Test 2 (dataset B, cell lattice of 1392x1040x1 voxels) with 142 227 voxels above the threshold and mean cluster volume of 1645 voxels, was 44 h. On the other hand, for Test 1 (dataset A, cell lattice of 692 $\times$ 520 $\times$ 1 voxels) with 171 607 voxels above the threshold and mean cluster volume of 1988 voxels, the simulation time was 8 d. Finally, the resizing of the same image led to a significant decrease in computation time. For instance, a resizing by a factor two in Test 5 (decreased in resolution from 0.62 nm/voxel to 1.24 nm/voxel) reduced the simulation time by a factor of 67 (from 201 h to 3 h) as compared to the non-resized image (Test 1). Thus, the minimum resolution of the generated geometries required for each study should be determined carefully for the sake of computational efficiency.

3.2. DSB distribution after MRT irradiation

Figure 4(b) Illustrates the MRT dose distributions at the cell lattice position and the derived spatial distribution of DSB in each cell nucleus of dataset C. As shown in figure 4(d), the spatial distribution of DSB per cell nucleus is highly heterogeneous following the heterogeneity of the dose distribution. In the peak dose region, defined as the volume receiving a dose higher than 50% of maximum, the average number of DSB per cell nucleus is 157 $\pm$ 28 (1 SD) (5.7 Gy per nucleus on average). The number of DSB in the dose fall-off

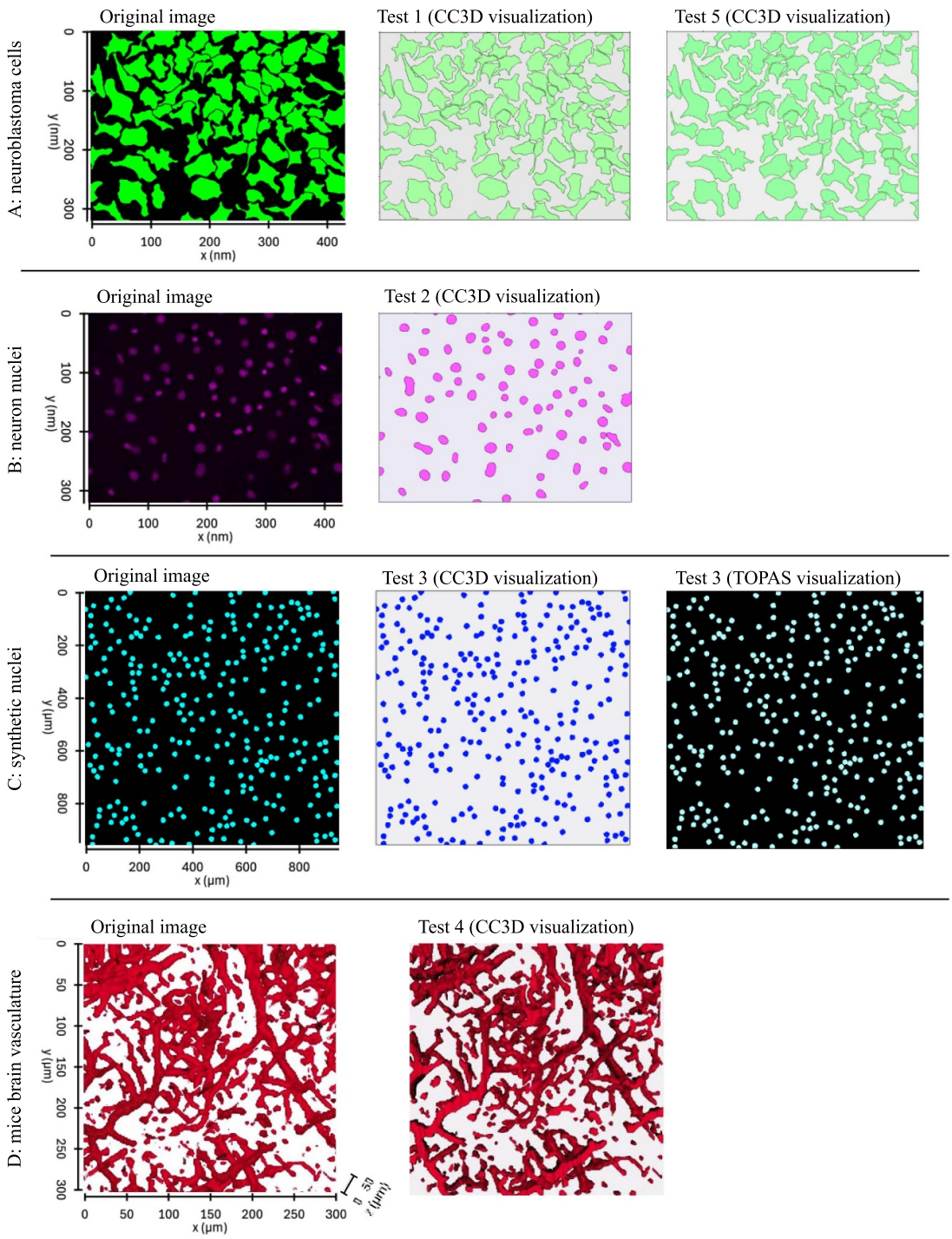

Figure 2. Original segmentation images and generated geometries. Each row contains one dataset (from A to D, see section 2.2), and the generated geometry in each of the test performed using each dataset. The images of the generated geometries were created using the CC3D visualization and, for Test 3, also using the TOPAS visualization.

Table 2. Dice similarity coefficient (DSC) between the original and generated geometries, and number of entities (i.e. cells or nuclei) in the original image and number of clusters in the generated PIF files, for the five tests performed.

Test #	1	2	3	4	5
Dataset	A	B	C	D	A
DSC	1.00	1.00	1.00	1.00	—
Original number of entities	87	87	300	—	87
Number of generated clusters	87	87	300	529	87

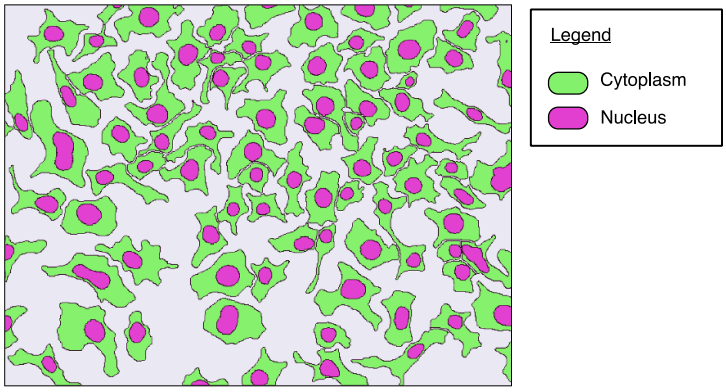

Figure 3. Cytoplasm and cell nucleus of neuroblastoma cells (dataset A) generated by the combination of two geometries created by the clustering tool. The image was generated using the generated PIF file in CC3D.

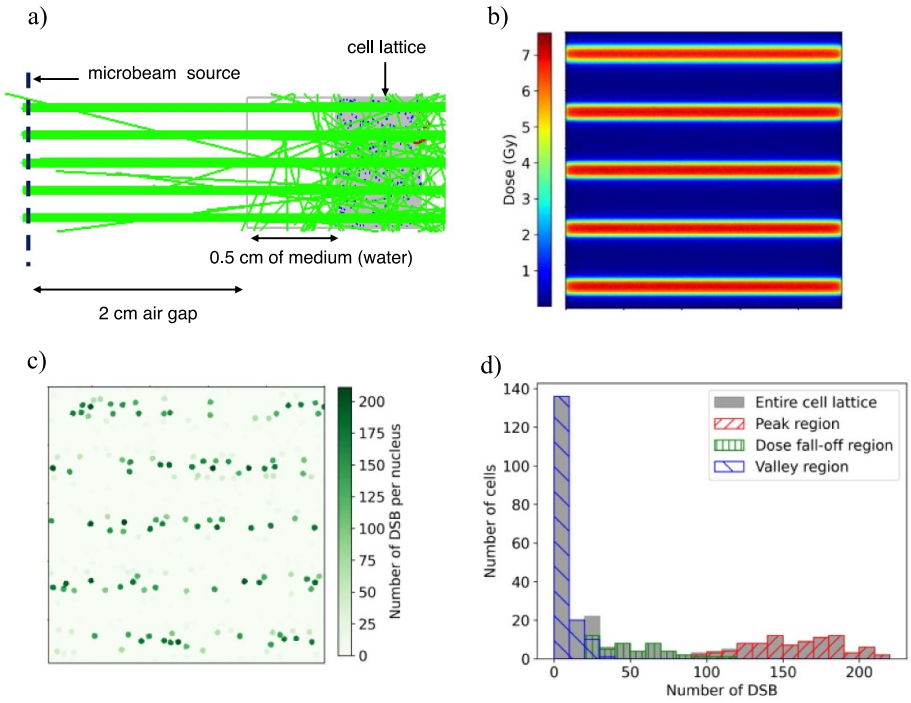

Figure 4. (a) Simulation setup in TOPAS, (b) MRT dose map, (c) DSB spatial distribution in the nuclei population of dataset C, and (d) distribution of DSB per nuclei at the entire cell lattice, and peak, dose fall off and valley regions.

region, i.e. volume receiving between 50% and 10% of the peak dose (1.9 Gy per nucleus on average), drops to 52 $\pm$ 21. Finally, the average number of DSB in the valley region, i.e. volume receiving less than 10% of the peak dose (0.2 Gy per nucleus Gy on average), is 6 $\pm$ 5. Figure 4(c) shows the distribution of the number of DSB per nuclei in the cell lattice considered (dataset C) at the peak, dose fall-off, and valley regions.

4. Discussion

The tool presented in this work aids in overcoming two of the main limitations in the creation of biological geometries in computational modeling for radiobiology research applications, i.e. the process of converting segmentation images into geometry formats for input in different simulations software, and the identification of voxels conforming individual biological entities.

First, it automatizes the process of converting voxel-based images into ready-to-use input files for the simulation of the transport of radiation in matter and the simulation of subsequent biological processes. The tool generates geometries in ImageCube and PIF formats, compatible with TOPAS and CC3D, two software dedicated to the Monte Carlo simulation of radiation transport and the modeling of radiochemical and biological processes, respectively. This automatic conversion prevents users from the need for coding to

perform this often-arduous conversion task, enabling its use by researchers with no coding experience. In addition, the creation of files with format readable by TOPAS and CC3D eases the interface between them.

Second, it automatically assigns a unique identifier to groups of image voxels, based on user-specifications, to create clusters to represent voxelized cells or subcellular geometries such as cellular nuclei for compartmental simulations. The impact in radiobiological modeling studies is as follows. (i) most of the associations of physical quantities (e.g. dose, LET, or microdosimetric quantities) with biological endpoints (e.g. induction of DSB, cell survival, or fraction of misrepair damage) are defined per cell or nucleus (Belov *et al* 2015, Thibaut *et al* 2023), and (ii) voxels associated to the same biological structure should behave in a coordinate manner as a single entity, for instance when simulating damage repair or mitosis processes. Thus, the identification and creation of these clusters (i.e. cells or cell nuclei) is required to perform computational radiobiological studies. The clustering process performed by this tool become even more significant when the individual entities are not discernible by eye in the images, for instance in segmentation images of the vasculature system, for which the survival of vascular cells can be associated with the dose per cell (Garcia-Barros *et al* 2003). The test performed in this work used four different image datasets of a wide variety of cell shapes and distributions (see figure 2) proving the versatility of the tool.

The tool developed in this work is expected to assist in computational modeling radiobiological studies which aim to reproduce specific geometries from experimental setups in terms of the spatial distribution of cells and their shape. This enables the modeling of specific biological processes and their validation using biological data from a specific experiment. Reproducing a specific geometries becomes more relevant when the agent that triggers the biological response (i.e. radiation) is not uniformly distributed since cell responses may depend on their topological shape and spatial position in the cell lattice. This is the case of several emergent radiotherapy techniques including Spatially Fractionated Radiation Therapy, where the radiobiological responses to the highly heterogeneous dose distributions are not fully described yet (Prezado *et al* 2024), theranostic, where the targeted accumulation of radioactive agents in specific cell compartments plays a relevant role in the cellular outcomes (Li *et al* 2022), or heavy ion therapy, where the energy deposition events are more densely distributed around the primary particle track, causing a non-uniformly damage distribution and triggering distinct repair mechanisms within a cell population (Asaithamby and Chen 2011).

As an example of the application of this tool, we simulated the spatial distribution of induced DSB in a cell population after x-ray MRT irradiation, which showed significant dependence on the cells position with respect to the radiation beams (see figure 4(c)). This proved the relevance of this tool for identifying the voxels conforming individual cells in scenarios where the dimension, shape and position of cells with respect the dose delivery pattern may influence the evaluation of a given biological endpoint. However, the radiobiological responses of tissues to MRT, discussed elsewhere in the literature (Prezado *et al* 2024), require a further investigation, which is out of the scope of this work.

In an ongoing work from our team, the clustering of voxels belonging to different cell compartments, e.g. cytoplasm and cell nucleus (see figure 3) is used to quantify the distinct free radical production and cytotoxicity in the different cell structures. This is possible due to the assignment of unique identifiers to the different compartments, which allows the definition of different materials, scavenging capacities, other physical or chemical properties to each structure, or biochemical processes (e.g. removal of long living reactive oxygen species like H_2O_2). Thus this tool is of relevance for disentangling the biochemical mechanism of FLASH radiotherapy (Favaudon *et al* 2014). Finally, the tool allowed identification of different cell structures which might facilitate the simulation setup of the intake and uptake of different radiopharmaceutical vectors in these cell compartments (Sgouros *et al* 2020) to mimic their selective accumulation in specific experimental setups.

This tool and the set of developed geometries will be available upon request to the corresponding author.

5. Conclusion

We developed a computational tool that performs the clustering of voxels of biological segmentation images to create biological structures (e.g. cells and nuclei) based on user-defined parameters. In addition, it converts the information contained in the images into file formats that allow importing the geometries into TOPAS and Compucell3D, software dedicated to the simulation of radiation transport and biological processes. Overall, this tool aims to ease the use of realistic biological geometries in computational radiobiological studies for the development of emerging radiotherapy techniques.

Data availability statement

All data that support the findings of this study are included within the article (and any supplementary information files).

Acknowledgments

This work was partially supported by the NIH/NCI RO1CA187003 and NIH/NCI R01CA266419 grants.

ORCID iDs

Ramon Ortiz https://orcid.org/0000-0002-4628-8121
José Ramos-Méndez https://orcid.org/0000-0002-8106-5142

References

Asaithamby A and Chen D J 2011 Mechanism of cluster DNA damage repair in response to high-atomic number and energy particles radiation *Mutat. Res.* **711** 87–99
Belov O V, Krasavin E A, Lyashko M S, Batmunkh M and Sweilam N H 2015 A quantitative model of the major pathways for radiation-induced DNA double-strand break repair *J. Theor. Biol.* **366** 115–30
Brodland G W 2015 How computational models can help unlock biological systems *Semin. Cell Dev. Biol.* **47–48** 62–73
Burger K *et al* 2017 Increased cell survival and cytogenetic integrity by spatial dose redistribution at a compact synchrotron x-ray source *PLoS One* **12** e0186005
Dice L R 1945 Measures of the amount of ecologic association between species *Ecology* **26** 3 297–302
Faddegon B A *et al* 2023 Ionization detail parameters and cluster dose: a mathematical model for selection of nanodosimetric quantities for use in treatment planning in charged particle radiotherapy *Phys. Med. Biol.* **68** 175013
Faddegon B, Ramos-Méndez J, Schuemann J, McNamara A, Shin J, Perl J and Paganetti H 2020 The TOPAS tool for particle simulation, a Monte Carlo simulation tool for physics, biology and clinical research *Phys. Med.* **72** 114–21
Favaudon V *et al* 2014 Ultrahigh dose-rate FLASH irradiation increases the differential response between normal and tumor tissue in mice *Sci. Trans. Med.* **6** 245ra93
Félétou M 2011 Introduction *The Endothelium: Part 1: Multiple Functions of the Endothelial Cells—Focus on Endothelium-Derived Vasoactive Mediators* (Morgan & Claypool Life Sciences) (available at: www.ncbi.nlm.nih.gov/books/NBK57145/) (Accessed 31 January 2024)
Garcia-Barros M, Paris F, Cordon-Cardo C, Lyden D, Rafii S, Haimovitz-Friedman A, Fuks Z and Kolesnick R 2003 Tumor response to radiotherapy regulated by endothelial cell apoptosis *Science* **300** 1155–9
Li W B, Bouvier-Capely C, Saldarriaga Vargas C, Andersson M and Madas B 2022 Heterogeneity of dose distribution in normal tissues in case of radiopharmaceutical therapy with alpha-emitting radionuclides *Radiat. Environ. Biophys.* **61** 579–96
Liu R, Higley K A, Swat M H, Chaplain M A J, Powathil G G and Glazier J A 2021 Development of a coupled simulation toolkit for computational radiation biology based on Geant4 and CompuCell3D *Phys. Med. Biol.* **66** 045026
McNamara A L *et al* 2018 Geometrical structures for radiation biology research as implemented in the TOPAS-nBio toolkit *Phys. Med. Biol.* **63** 175018
Perl J, Shin J, Schumann J, Faddegon B and Paganetti H 2012 TOPAS: an innovative proton Monte Carlo platform for research and clinical applications *Med. Phys.* **39** 6818–37
Prezado Y, Grams M, Jouglar E, Martínez-Rovira I, Ortiz R, Seco J and Chang S 2024 Spatially fractionated radiation therapy: a critical review on current status of clinical and preclinical studies and knowledge gaps *Phys. Med. Biol.* **69** 10TR02
Ramos-Méndez J *et al* 2021 TOPAS-nBio validation for simulating water radiolysis and DNA damage under low-LET irradiation *Phys. Med. Biol.* **66** 175026
Rothkamm K and Löbrich M 2003 Evidence for a lack of DNA double-strand break repair in human cells exposed to very low x-ray doses *Proc. Natl Acad. Sci.* **100** 5057–62
Ruusuvuori P 2011 CIL:27852 *CIL* (available at: http://cellimagelibrary.org/images/27852) (Accessed 19 June 2024)
Schuemann J, McNamara A L, Ramos-Méndez J, Perl J, Held K D, Paganetti H, Incerti S and Faddegon B 2018 TOPAS-nBio: an Extension to the TOPAS Simulation Toolkit for Cellular and Sub-cellular Radiobiology *Rare* **191** 125–38
Sgouros G, Bodei L, McDevitt M R and Nedrow J R 2020 Radiopharmaceutical therapy in cancer: clinical advances and challenges *Nat. Rev. Drug Discov.* **19** 589–608
Slatkin D N, Spanne P, Dilmanian F A and Sandborg M 1992 Microbeam radiation therapy *Med. Phys.* **19** 1395–400
Swat M H, Thomas G L, Belmonte J M, Shirinifard A, Hmeljak D and Glazier J A 2012 Multi-scale modeling of tissues using CompuCell3D *Methods Cell Biol.* **110** 325–66
Thibaut Y, Gonon G, Martinez J S, Petit M, Vaurijoux A, Gruel G, Villagrasa C, Incerti S and Perrot Y 2023 MINAS TIRITH: a new tool for simulating radiation-induced DNA damage at the cell population level *Phys. Med. Biol.* **68** 034002
Todorov M I *et al* 2020 Machine learning analysis of whole mouse brain vasculature *Nat. Methods* **17** 442–9
Weimiao Yu H K L 2019 CCDB:6843 *CIL* (https://doi.org/10.7295/W9CCDB6843)
Zhang H and Mayr N A (ed) 2023 *Spatially Fractionated, Microbeam and FLASH Radiation Therapy. In 2053–2563* (IOP Publishing) (https://doi.org/10.1088/978-0-7503-4046-5)
Zou K H, Warfield S K, Bharatha A, Tempany C M C, Kaus M R, Haker S J, Wells W M, Jolesz F A and Kikinis R 2004 Statistical validation of image segmentation quality based on a spatial overlap index *Acad. Radiol.* **11** 178–89